Mon. Not. R. Astron. Soc. **364,** 934–942 (2005) doi:10.1111/j.1365-2966.2005.09622.x

The effect of neutrinos on the initial fireballs in gamma-ray bursts

Hylke B. J. Koers[1,2]★ and Ralph A. M. J. Wijers[3]★

[1]*NIKHEF, PO Box 41882, 1009 DB Amsterdam, the Netherlands*
[2]*University of Amsterdam, Amsterdam, the Netherlands*
[3]*Astronomical Institute 'Anton Pannekoek', Faculty of Science, University of Amsterdam, Kruislaan 403, 1098 SJ Amsterdam, The Netherlands*

Accepted 2005 September 19. Received 2005 June 1

ABSTRACT

We investigate the fate of very compact, sudden energy depositions that may lie at the origin of gamma-ray bursts (GRBs). Following on from the work of Cavallo & Rees, we take account of the much higher energies now believed to be involved. The main effect of this is that thermal neutrinos are present and energetically important. We show that these may provide sufficient cooling to tap most of the explosion energy. However, at the extreme energies usually invoked for GRBs, the neutrino opacity suffices to prevent dramatic losses, provided that the heating process is sufficiently fast. In a generic case, a few tens of per cent of the initial fireball energy will escape as an isotropic millisecond burst of thermal neutrinos with a temperature of about 60 MeV, which is detectable for nearby GRBs and hypernovae. For parameters we find most likely for GRB fireballs, the dominant processes are purely leptonic and thus the baryon loading of the fireball does not affect our conclusions.

Key words: neutrinos – gamma-rays: bursts.

1 INTRODUCTION

Due to their tremendous energy, and in view of the connections discovered in recent years between gamma-ray bursts (GRBs) and massive stars (e.g. Van Paradijs, Kouveliotou & Wijers 2000 and references therein), it is now generally assumed that a GRB is initiated when a few solar masses of material collapse to near their Schwarzschild radius. In the simplest possible models of what happens next, a fair fraction of the gravitational energy released in the collapse is deposited into a volume somewhat larger than that of the horizon of the collapsed mass. The subsequent evolution of such a volume of highly concentrated energy (termed 'fireball') was explored by Cavallo & Rees (1978). These authors introduced a compactness parameter for the volume, which expresses how easily a plasma consisting of baryons, photons, electrons and positrons can emit energy within a dynamical time. For small compactness, the emission is easy and the fireball cools by radiation. For large compactness, photons are trapped and cooling occurs by adiabatic expansion: an explosion results in which a significant fraction of the initial fireball energy is converted to bulk kinetic energy of a relativistic outflow, a condition now thought necessary for producing a GRB.

At the time, Cavallo and Rees considered still relatively nearby origins of GRBs, for which the required fireball energies imply conditions that justified their assumption for the fireball composition. However, with cosmological distances to GRBs, the required fireball energies are now so large that conditions of copious neutrino production become quite plausible. Motivated by the concern that these neutrinos easily leave their creation site due to their weak interaction with matter and thereby carry away enough energy to weaken or prevent an explosion, we investigate the evolution of neutrino-rich fireballs. Neutrino emission was previously considered as a sink of fireball energy, e.g. by Kumar (1999), who included emission of neutrinos in the optically thin limit. Neutrino emissivity has been more widely studied in a slightly different context, namely the evolution post-collapse of the accretion disc or torus around the newborn black hole, which may tap the accretion energy of the torus to power a GRB (Woosley 1993). The effect of neutrino opacity in this process has been the subject of a few recent studies, e.g. by Janiuk et al. (2004) and by Lee, Ramirez-Ruiz & Page (2004).

Here, we study the evolution of a spherical fireball with given initial radius, energy and baryon content. We aim to be general in the physical processes we consider, but accept a few a priori constraints on the initial parameters of the fireball: its initial energy must suffice to power a GRB, hence it should be within a few decades of 10^{52} erg; its initial size cannot be much larger than the Schwarzschild radius of a few solar masses, say $10^{6.5}$ cm, because the mass must collapse to such small radii in order to liberate such a large energy. Lastly, the initial ratio of fireball energy to rest mass, M_0, of the entrained baryons, $\eta \equiv \mathcal{E}/M_0c^2$, must be several hundred (corresponding to almost 1 TeV baryon^{-1}) in order that eventually the baryons may be accelerated to a Lorentz factor high enough to produce a GRB. This combination of constraints implies that the fireballs we study here are always very compact in the Cavallo and Rees (or electromagnetic) sense. It also implies, as we show here, that the baryons are relatively unimportant in the neutrino processes.

★E-mail: hkoers@nikhef.nl (HBJK); rwijers@science.uva.nl (RAMJW)

This paper is organized as follows: in Section 2, we discuss some general properties of the fireball environment. Using these, we investigate the most important neutrino interactions in this environment in Section 3. We introduce the emissivity parameter χ and the optical depth τ to describe the neutrino physics and we present a phase diagram for the neutrino fireball. The dynamical evolution of the neutrino fireball is discussed in Section 4. The neutrino emission is discussed in Section 5 and we present our conclusions in Section 6.

2 GENERAL PROPERTIES

2.1 Composition and temperature

The term 'fireball' refers to a plasma consisting of photons, electrons and positrons, possibly with a small baryonic load (Cavallo & Rees 1978). In this paper, we extend this to fireballs that contain neutrinos.[1] We consider a fireball that is initially opaque to neutrinos of all flavours. At some point during the expansion of the fireball (to be discussed in Section 4.2), it becomes transparent to muon- and tau-neutrinos, that subsequently decouple from the plasma. The electron-neutrinos decouple a bit later, which divides the plasma parameter space into three regions: region I where the fireball contains neutrinos of all flavours; region II where it contains only electron-neutrinos; and region III where all the neutrinos are decoupled.

In thermodynamic equilibrium, the energy density and temperature are related by

$$\frac{\mathcal{E}}{V} = gaT^4 \,, \tag{1}$$

where a is the radiation constant and g is a pre-factor that depends on the composition of the system. For the three regions introduced above:

$$g_{\rm I} = \frac{43}{8} \,, \qquad g_{\rm II} = \frac{29}{8} \,, \qquad g_{\rm III} = \frac{22}{8} \,. \tag{2}$$

Assuming a spherical configuration, the temperature of the plasma can be expressed in terms of the energy and radius as

$$(T_{11})^4 = \frac{100}{g} \, (\mathcal{E}_{52}) \, (R_{6.5})^{-3} \,, \tag{3}$$

where $T = T_{11} \times 10^{11}\,{\rm K}$, $\mathcal{E} = \mathcal{E}_{52} \times 10^{52}\,{\rm erg}$ and $R = R_{6.5} \times 10^{6.5}\,{\rm cm}$.

We use the following values for the initial fireball energy and radius as a reference (denoted with an asterisk):

$$\mathcal{E}_* = 10^{52}\,{\rm erg} \,, \tag{4a}$$

$$R_* = 10^{6.5}\,{\rm cm} \,. \tag{4b}$$

The reference temperature is

$$T_* = 2.1 \times 10^{11}\,{\rm K} = 17.9/k_{\rm B}\,{\rm MeV} \,. \tag{4c}$$

2.2 Baryons

As the temperature is higher than typical binding energies, nuclei are dissociated into nucleons. Hence, 'baryons' means 'nucleons' in what follows ('baryon' is however the standard terminology). The requirement that there should be 1 TeV of energy available for the baryons leads to a maximum number density of

$$n_{\rm B,*} = 4.7 \times 10^{31}\,{\rm cm}^{-3} \,, \tag{5}$$

which will be used as the reference value in this study. It implies a baryonic mass density of $\rho_{\rm B,*} = 9.4 \times 10^7\,{\rm gr\,cm}^{-3}$, which corresponds to a total baryonic mass of 6.2×10^{-6} solar masses contained in the volume V_*. Note that the nucleons are non-degenerate.

Because of overall charge neutrality, the ratio of protons to neutrons can be expressed in terms of the electron fraction $Y_{\rm e}$:

$$n_{\rm B} = n_{\rm n} + n_{\rm p} \,, \tag{6a}$$

$$n_{\rm p} = Y_{\rm e} n_{\rm B} = \Delta n_{\rm e} \,, \tag{6b}$$

where $\Delta n_{\rm e} = n_{\rm e^-} - n_{\rm e^+}$ is the net electron density. The exact value of $Y_{\rm e}$ in a physical situation is determined by beta-equilibrium conditions; see e.g. Bethe, Applegate & Brown (1980) and Beloborodov (2003). As we will see in the next section, the exact value of $Y_{\rm e}$ is not very important for our purposes.

2.3 Electron and positron number densities

Because $T_* \gg m_{\rm e}c^2$, the electrons and positrons are extremely relativistic. Using $E = pc$, the net electron density and the combined electron–positron density $n_{\rm e} = n_{\rm e^-} + n_{\rm e^+}$ can be expressed as

$$\Delta n_{\rm e} = \frac{1}{3\hbar^3 c^3} \left[(k_{\rm B}T)^2 \mu_{\rm e} + \frac{{\mu_{\rm e}}^3}{\pi^2} \right] \,, \tag{7a}$$

$$n_{\rm e} = 0.37 \frac{(k_{\rm B}T)^3}{\hbar^3 c^3} + \mathcal{O}\,(\mu_{\rm e})^2 \,, \tag{7b}$$

where $\mu_{\rm e}$ is the electron chemical potential.

By definition, $Y_{\rm e} < 1$, so that $\Delta n_{\rm e} \leqslant n_{\rm B}$. This places an upper bound on the net electron density and, through equation (7a), on the electron chemical potential. With the reference baryon number density of equation (5), we find that the electron chemical potential is very small: $\mu_{\rm e}/(k_{\rm B}\,T_*) \sim 2 \times 10^{-4} \ll 1$. From (7b), neglecting the chemical potential, we find that at the reference temperature T_*:

$$n_{\rm e^-,*} = n_{\rm e^+,*} = 1.4 \times 10^{35}\,{\rm cm}^{-3} \,. \tag{8}$$

Concluding, the fireball under consideration here is nucleon-poor ($n_{\rm B} \ll n_{\rm e}$) and has a very small electron chemical potential ($\Delta n_{\rm e} \ll n_{\rm e}$). This implies that the electrons and positrons are non-degenerate.

3 FIREBALL NEUTRINO PHYSICS

3.1 The dominant neutrino processes

The relative importance of interactions between neutrinos and the other components of the plasma depends on the temperature, the electron chemical potential and the baryon density. The most important neutrino production processes are discussed in Appendix A1. Scattering and absorption processes are discussed in Appendix B. We use the fact that nucleons, electrons and positrons are non-degenerate.

For the present baryon densities, we observe from Figs A1 and B1 that for temperatures $T > 5 \times 10^{10}\,{\rm K}$, the neutrino physics is dominated by leptonic processes. The dominant neutrino production process is electron–positron pair annihilation:

$$\mathrm{e}^- + \mathrm{e}^+ \rightarrow \nu + \bar{\nu} \,, \tag{9}$$

[1] Unless the difference is important, we will use the word 'neutrinos' if we mean 'neutrinos and antineutrinos'.

and the neutrino mean free path (mfp) length is set by scattering off electrons and positrons:

$$\nu + e^{\pm} \rightarrow \nu + e^{\pm} \tag{10}$$

and similar for antineutrinos.

As the initial temperature of the fireball is high ($T_0 \sim 2 \times 10^{11}$ K), we will only consider these processes in the following.

3.2 Neutrino creation rate

We express the neutrino creation rate in terms of the parameter $\chi = t_c/t_e$, where $t_c = \mathcal{E}/(VQ)$ is the cooling time-scale and $t_e = R/c_s$ is the expansion time-scale (c_s is the sound speed in the fireball). This parameter bears no reference to the neutrino transparency of the plasma, which has to be taken into account if one considers cooling by neutrino emission. The emissivity of electron–positron pair annihilation is (see Appendix A1)

$$Q_{\rm pair} = 3.6 \times 10^{33}\ (T_{11})^9\ {\rm erg\,s^{-1}\,cm^{-3}}\,. \tag{11}$$

Because Q is a function of temperature, it depends on the size, energy and composition of the fireball through equation (3). It follows that

$$\chi = 3.7 \times 10^{-3}\, g^{9/4}\, (\mathcal{E}_{52})^{-5/4}\, (R_{6.5})^{11/4}\ , \tag{12}$$

where we used $c_s = c/\sqrt{3}$. For the reference values $\mathcal{E}_0 = 10^{52}$ erg and $R_0 = 10^{6.5}$ cm, we find that $\chi_{\rm I} = 0.16$, which means that neutrinos are created reasonably rapidly as compared with the expansion time-scale. Neutrinos and antineutrinos are created in pairs by electron–positron annihilation, so they will be present in equal amounts.[2]

A different source of neutrinos is the decay of charged pions due to photo-pion production (see Appendix A2) by high-energy photons ($E_\gamma > 140$ MeV). The energy stored in the high-energy tail of the photon distribution is relatively small (∼5 per cent). The process manifests itself as a high-energy leak, resulting in an increased production of electron- and muon-neutrinos with energies below $m_\mu/2 \simeq 53$ MeV. We will not consider this non-thermal process in the rest of this paper.

3.3 Optical depth

The opacity of the fireball to neutrinos is described in terms of the optical depth $\tau = R/\lambda$, where R is the length scale and λ is the mfp. The mfp due to electron and positron scattering is (see Appendix B1)

$$\lambda^{(e)} = 3.7 \times 10^6\ (T_{11})^{-5}\ {\rm cm}\,, \tag{13a}$$

$$\lambda^{(\mu,\tau)} = 1.6 \times 10^7\ (T_{11})^{-5}\ {\rm cm}\,, \tag{13b}$$

where the difference originates from the fact that only electron-neutrinos participate in charged current-interactions. Because the mfp for neutrinos and antineutrinos is equal (assuming an equal amount of electrons and positrons), neutrinos and antineutrinos will leave the fireball at the same time.

We consider a generic plasma that moves from region I to II to III. Therefore, we use the value $g = g_{\rm I}$ to find the optical depth for the muon- and tau-neutrinos and $g = g_{\rm II}$ for the electron-neutrinos:

$$\tau^{(e)} = 54 \times (\mathcal{E}_{52})^{5/4}\, (R_{6.5})^{-11/4}\ , \tag{14a}$$

$$\tau^{(\mu,\tau)} = 7.4 \times (\mathcal{E}_{52})^{5/4}\, (R_{6.5})^{-11/4}\ . \tag{14b}$$

[2] This conclusion changes if there is an initial asymmetry between neutrinos and antineutrinos. We do not consider this here.

We observe that, for reference initial conditions, $\tau^{(e,\mu,\tau)} > 1$ so that the fireball is opaque to neutrinos of all flavours.

3.4 Phases of the neutrino fireball

We will assume that neutrinos of some flavour decouple from the plasma instantaneously if the optical depth is one (these transitions will be smoother in reality). Based on equation (14), Fig. 1 shows how the parameter space is divided into the regions I, II and III by the $\tau^{(\mu,\tau)} = 1$ and $\tau^{(e)} = 1$ contours. The dynamical evolution of a fireball through these regions will be discussed in Section 4.2.

We observe that the region of interest has a temperature $T > 5 \times 10^{10}$ K, which justifies the fact that we only consider electron–positron pair annihilation and neutrino scattering off electrons and positrons (see Figs A1 and B1).[3]

The figure also indicates the neutrino creation rate from equation (12). In region I, this process is fast compared with the expansion time-scale. Together with the reverse process, it aims towards thermodynamic equilibrium between the neutrinos and the other components of the plasma. The neutrinos also interact with the electrons and positrons through scattering. The interaction length of this process is smaller than the size of the fireball. We conclude that thermodynamic equilibrium is established rapidly and the system will remain in equilibrium throughout its evolution.

4 FIREBALL EVOLUTION

4.1 Hydrodynamics

As long as the components of the plasma are strongly coupled (i.e. the interaction length is much smaller than the size of the system), the plasma can be described as a homogeneous sphere, in thermodynamic equilibrium with a single temperature. The evolution will be very similar to that of a neutrinoless fireball as described by e.g. Shemi & Piran (1990). The plasma expands by radiation pressure, converting radiative energy to kinetic energy of the baryons. We assume that the expansion is adiabatic. We will denote the radiative energy contained in the fireball (without the decoupled components) as $\mathcal{E}$. The energy and entropy within a sphere of radius R are

$$\mathcal{E} = \frac{4\pi}{3} g a R^3 T^4\,, \tag{15a}$$

$$S = \frac{16\pi}{9} g a (RT)^3\,. \tag{15b}$$

Assuming that the evolution of the fireball is reversible (i.e. entropy is conserved), the temperature–radius relationship reads

$$g(RT)^3 = g_0(R_0T_0)^3 = \text{constant}. \tag{16}$$

As long as there is no change in the plasma composition, the following very useful scaling laws can be used to describe the evolution (Shemi & Piran 1990):

$$\mathcal{E}R = \mathcal{E}_0 R_0 = \text{constant}, \tag{17a}$$

$$\frac{\mathcal{E}}{T} = \frac{\mathcal{E}_0}{T_0} = \text{constant}. \tag{17b}$$

[3] Nuclear processes become competitive with the leptonic processes at these temperatures if the nucleon density is approximately 2 orders of magnitude higher. In that case, the optical depth- and emissivity-lines in Fig. 1 feature a bend at a cross-over temperature.

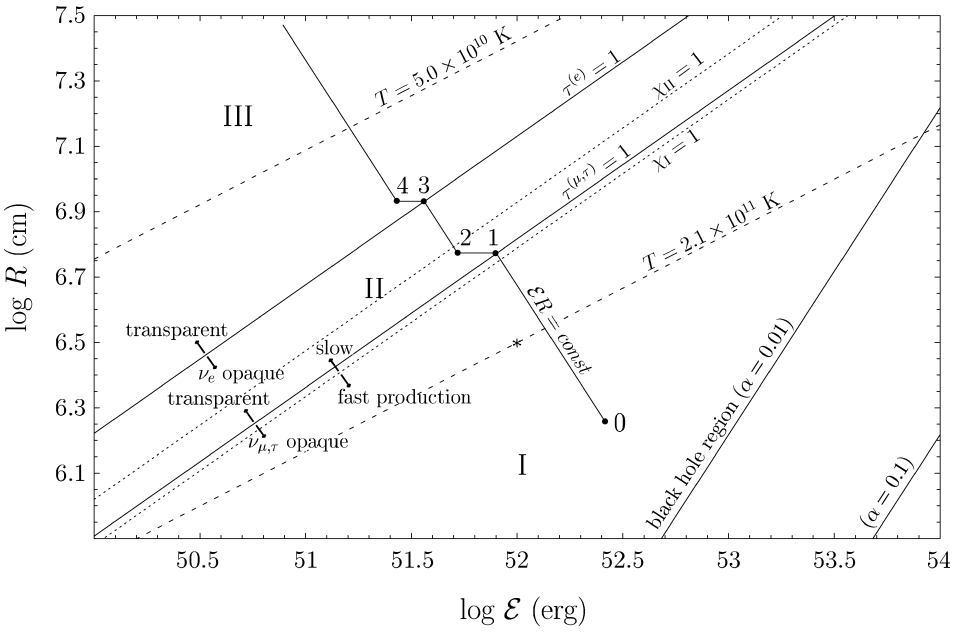

Figure 1. A parameter space plot that shows the three phases of the plasma. The solid lines show the $\chi_{\rm I} = 1$, $\chi_{\rm II} = 1$, $\tau^{(\mu,\tau)} = 1$ and $\tau^{(\rm e)} = 1$ contours; the dotted lines are isotemperature curves. The $*$ denotes the reference point with values given in equation (4). The plotted trajectory and the points '0' to '4' are discussed in Section 4.2. The black hole lines indicate the Schwarzschild radius as a function of the fireball energy, assuming an initial conversion efficiency $\alpha = E^{(0)}/M_{\rm BH}c^2$.

If a plasma component annihilates, the temperature–radius relationship (16) still holds by conservation of entropy. In the early universe, this leads to an increase in the photon temperature after electron–positron annihilation (see e.g. Weinberg 1972) and a similar effect happens in the last stage of the neutrinoless fireball (Shemi & Piran 1990). By contrast, entropy is carried away if a component decouples:

$$S = S_0 - S_{\rm dec}\,, \tag{18}$$

where $S_{\rm dec}$ is the entropy in the decoupled components. Because $g = g_0 - g_{\rm dec}$, it follows from equation (15) that the temperature–radius relationship does not change at decoupling:

$$RT = R_0 T_0\,. \tag{19}$$

4.2 Neutrino decoupling bursts

We will discuss the hydrodynamical evolution of a fireball that starts in region I with a generic initial energy $\mathcal{E}_0$ and size R_0. The trajectory is sketched in Fig. 1. As the fireball expands and cools, it will develop from neutrino-opaque to -transparent. When this happens, neutrinos decouple from the plasma.

Apart from these bursts, neutrinos are emitted continuously in regions where the creation rate is sufficiently high and the plasma is transparent to neutrinos. We will consider this in more detail in Section 4.3 and restrict our discussion to an expanding fireball with events of instantaneous energy loss here.

Starting from the point denoted as '0' in Fig. 1, the plasma expands along a $\mathcal{E}R = \mathcal{E}_0 R_0$ line until it reaches the $\tau^{(\mu,\tau)} = 1$ contour, where the muon- and tau-neutrinos decouple from the plasma. From equation (14b), we find that the radiative energy and temperature of the plasma just before decoupling are

$$\mathcal{E}_{52}^{(1)} = 0.61\left[\mathcal{E}_{52}^{(0)}\,R_{6.5}^{(0)}\right]^{11/16}\,, \tag{20a}$$

$$T_{11}^{(1)} = 1.26\left[\mathcal{E}_{52}^{(0)}\,R_{6.5}^{(0)}\right]^{-1/16}\,. \tag{20b}$$

The temperature of the plasma at that point depends on the initial conditions only very mildly, but it is interesting that the temperature of the plasma at decoupling is lower if the initial energy is higher. This can be seen from Fig. 1: for a higher $\mathcal{E}_0$, the $\mathcal{E}R =$ constant line crosses the $\tau^{(\mu,\tau)} = 1$ contour at a lower temperature. The muon- and tau-neutrinos carry away $14/43 \simeq 33$ per cent of the available radiative energy. This moves the fireball from point 1 to point 2.

Because the size and temperature of the plasma are constant at decoupling, what remains of the fireball continues adiabatic expansion along a new trajectory. The electron-neutrinos remain in thermal equilibrium with the plasma, which enters region II. The expansion continues along a $\mathcal{E}R = \mathcal{E}_2 R_2$ curve until the plasma becomes transparent to electron-neutrinos at $\tau^{(\rm e)} = 1$ (point 3):

$$\mathcal{E}_{52}^{(3)} = 0.28\left[\mathcal{E}_{52}^{(0)}\,R_{6.5}^{(0)}\right]^{11/16}\,, \tag{21a}$$

$$T_{11}^{(3)} = 0.87\left[\mathcal{E}_{52}^{(0)}\,R_{6.5}^{(0)}\right]^{-1/16}\,. \tag{21b}$$

At this point, the electron-neutrinos leave the plasma and carry away $7/29 \simeq 24$ per cent of the energy (point 4). When all the neutrinos are decoupled, the fireball will develop according to the standard scenario (Shemi & Piran 1990).

The energy that is emitted in neutrinos in the two bursts is

$$E_{52}^{(\nu\text{bursts})} = \frac{14}{43}\mathcal{E}_{52}^{(1)} + \frac{7}{29}\mathcal{E}_{52}^{(3)} = 0.27\left[\mathcal{E}_{52}^{(0)}\,R_{6.5}^{(0)}\right]^{11/16}\,, \tag{22}$$

which is a significant fraction of the initial radiative energy.

4.3 Continuous neutrino cooling

In regions in the parameter space where the neutrino creation rate is high ($\chi \lesssim 1$) and (some of) the neutrinos can escape from the plasma ($\tau \lesssim 1$), we should take neutrino cooling into account in the hydrodynamical evolution.

A plasma expanding adiabatically along a $\mathcal{E}R = \text{constant}$ contour converts radiative energy to kinetic energy according to

$$\left.\frac{\mathrm{d}\mathcal{E}}{\mathrm{d}R}\right|_{\text{exp}} = -\frac{\mathcal{E}}{R}\,. \tag{23}$$

To this, we add the energy loss by neutrino cooling $\Delta\mathcal{E} = -fQV\Delta t$, where Q is the emissivity and f is the fraction of the created neutrinos that can leave the plasma. Assuming $\Delta R \simeq c_\mathrm{s}\,\Delta t$, we find that

$$\left.\frac{\mathrm{d}\mathcal{E}}{\mathrm{d}R}\right|_{\nu\text{cooling}} \simeq -\frac{fQV}{c_\mathrm{s}} = -\frac{f}{\chi}\frac{\mathcal{E}}{R}\,, \tag{24}$$

where $\chi = \chi(\mathcal{E}, R)$ is the creation rate as defined in Section 3.2. The plasma evolution, including neutrino cooling, can then be determined from the differential equation

$$\frac{\mathrm{d}\mathcal{E}}{\mathrm{d}R} = -\left(1+\frac{f}{\chi}\right)\frac{\mathcal{E}}{R}\,, \tag{25}$$

so that, locally, the plasma moves along a $\mathcal{E}R^{1+f/\chi} = \text{constant}$ trajectory. From equation (12), we find that, just after electron- and muon-neutrino decoupling, the creation rate parameter is

$$\chi_\mathrm{II} = 0.81\,, \tag{26}$$

independent of initial conditions. Hence, the creation rate is reasonably high in this region, where only muon- and tau-neutrinos can escape. Using the emissivity formulae from Munakata, Kohyama & Itoh (1985), we find that 31 per cent of the neutrinos created by electron–positron pair creation are muon- or tau-neutrinos, so that $f = 0.31$. Combining this with equations (12) and (25), we find that the plasma expands until it reaches the $\tau^{(\mathrm{e})} = 1$ contour at

$$\mathcal{E}_{52}^{(3)} = 0.27\left[\mathcal{E}_{52}^{(0)}\,R_{6.5}^{(0)}\right]^{11/16}\,, \tag{27a}$$

$$T_{11}^{(3)} = 0.89\left[\mathcal{E}_{52}^{(0)}\,R_{6.5}^{(0)}\right]^{-1/16}\,, \tag{27b}$$

which are almost identical to equations (21a) and (21b), respectively.

After electron-neutrino decoupling, neutrinos of all flavours can leave the plasma. The energy loss due to continuous neutrino cooling in regions II and III is

$$E_{52}^{(\nu,\mathrm{II})} = 0.027\left[\mathcal{E}_{52}^{(0)}\,R_{6.5}^{(0)}\right]^{11/16}\,, \tag{28a}$$

$$E_{52}^{(\nu,\mathrm{III})} = 0.015\left[\mathcal{E}_{52}^{(0)}\,R_{6.5}^{(0)}\right]^{11/16}\,. \tag{28b}$$

The continuous energy loss component is relatively small and hardly affects the fireball evolution. In particular, neutrino cooling is never efficient enough to prevent a hot fireball from exploding.

5 NEUTRINO EMISSION

5.1 Observed temperature

For the neutrinoless fireball, it is well known that the temperature of the observed photon spectrum is roughly equal to the initial temperature of the plasma T_0 (Goodman 1986; Shemi & Piran 1990). Let us recall the thermodynamic treatment of this phenomenon (Goodman 1986). The number of photons in a sphere of radius R depends on the temperature T as

$$N_\gamma = \frac{2\zeta(3)}{\pi^2}\left(\frac{k_\mathrm{B}T}{\hbar c}\right)^3\left(\frac{4}{3}\pi R^3\right) \sim 1.0\left(\frac{k_\mathrm{B}}{\hbar c}\right)^3 (RT)^3\,. \tag{29}$$

As long as none of the plasma components annihilates, the number of photons is constant during the evolution. The average available energy per photon for a neutrinoless fireball is initially

$$\langle E_\gamma\rangle^{(0)} = \frac{4}{11}\frac{E_\mathrm{tot}}{N_\gamma^{(0)}}\,. \tag{30}$$

Because the total energy is conserved, the available energy per photon does not change during the evolution of the fireball.

This conclusion is unaffected by the annihilation of electrons and positrons that occurs in the last stage of the fireball: entropy conservation requires that the number of photons increases by a factor of 11/4. However, the total energy is now exclusively available for the photons, so the available energy increases by the same factor. The mean photon energy does not change during the evolution of the neutrinoless fireball and the observed photon spectrum is roughly equal to the initial blackbody (Goodman 1986), with temperature (Shemi & Piran 1990; Piran, Shemi & Narayan 1993)

$$T_\mathrm{obs} = \gamma T \simeq T^{(0)}\,. \tag{31}$$

As for photons, the mean available energy for muon- and tau-neutrinos remains constant during the expansion from point 0 to 1, so the observed temperature will roughly equal the initial temperature.

For the electron-neutrinos, the situation is more subtle because energy leaves the plasma when the muon- and tau-neutrinos decouple. Initially, the mean available energy is

$$\langle E_{\nu_\mathrm{e}}\rangle^{(0)} = \frac{7}{43}\frac{E_\mathrm{tot}}{N_{\nu_\mathrm{e}}^{(0)}}\,, \tag{32}$$

which remains constant throughout the evolution to point 1. At point 2, the available energy is reduced by a factor 29/43, but the electron-neutrinos get a larger share:

$$\langle E_{\nu_\mathrm{e}}\rangle^{(2)} = \frac{7}{29}\frac{\frac{29}{43}E_\mathrm{tot}}{N_{\nu_\mathrm{e}}^{(2)}} = \langle E_{\nu_\mathrm{e}}\rangle^{(0)}\frac{N_{\nu_\mathrm{e}}^{(0)}}{N_{\nu_\mathrm{e}}^{(2)}}\,. \tag{33}$$

The number of neutrinos[4] in a sphere of radius R is proportional to $(RT)^3$. Because $R_2T_2 = R_1T_1 = R_0T_0$, the mean available energy does not change when some plasma components decouple. We conclude that the observed temperature of the electron-neutrino spectrum is also approximately equal to $T^{(0)}$.

5.2 Energy

The evolution of a fireball with neutrinos is described in Section 4. Using the results obtained in equations (22) and (28), we summarize the neutrino emission in Table 1. Neutrinos and antineutrinos are emitted in equal amounts and share the energy quoted in the table. The total energy that is emitted in neutrinos equals

$$E^{(\nu,\,\mathrm{tot})} = 3.1\times10^{51}\,\mathrm{erg}\times\left[E_{52}^{(0)}R_{6.5}^{(0)}\right]^{11/16}\,. \tag{34}$$

The mean neutrino energy follows directly from the initial temperature:

$$\langle E_\nu\rangle = 3.15k_\mathrm{B}T^{(0)} = 56\,\mathrm{MeV}\times\left[E_{52}^{(0)}\right]^{1/4}\left[R_{6.5}^{(0)}\right]^{-3/4}\,. \tag{35}$$

[4] This is similar to equation (29), but for neutrinos (one flavour) the pre-factor is 0.38 rather than 1.0.

Table 1. The total energy that is emitted in neutrinos in various stages. Here, 'dec.' stands for decoupling bursts and 'cont.' for continuous emission. The symbol ν means 'neutrino and antineutrino' in the above, and $\xi_0 := [E_{52}^{(0)}\, r_{6.5}^{(0)}]^{11/16}$.

	$E_{52}^{(\nu\,\mathrm{tot})}$	ν_e :	ν_μ :	ν_τ
$\nu_{\mu,\tau}$ dec.	$0.20 \times \xi_0$	0	0.5	0.5
ν_e dec.	$0.070 \times \xi_0$	1	0	0
Cont. II	$0.024 \times \xi_0$	0	0.5	0.5
Cont. III	$0.013 \times \xi_0$	0.69	0.15	0.15
Total	$0.31 \times \xi_0$	0.26	0.37	0.37

5.3 Time spread

The neutrinos are emitted in two decoupling bursts as well as continuously. As is clear from Fig. 1, the fireball has not expanded much in between the two decoupling events: $R^{(1)} - R^{(3)} \sim R^{(1)}$, implying that the various components of neutrino emission overlap in time. The intrinsic time spread is determined by the size of the fireball at the second burst:

$$\Delta t = \frac{R^{(3)}}{c} \sim 0.4\,\mathrm{ms} \times R_{6.5}^{(0)}\,, \tag{36}$$

which is much smaller than the typical time spread for supernova neutrinos that originate from relatively slow deleptonization processes.

Dispersion effects on the way to Earth introduce an additional smearing:

$$\Delta t_\mathrm{disp} = \frac{D}{c}\left(\frac{1}{\beta} - 1\right) = 0.6\,\mathrm{ms} \times \left(\frac{m_\nu}{0.1\,\mathrm{eV}}\right)^2 \left(\frac{E_\nu}{56\,\mathrm{MeV}}\right)^{-2} \left(\frac{D}{4\,\mathrm{Mpc}}\right)^2 . \tag{37}$$

For a robust analysis, this time spread should be averaged over a thermal distribution.

5.4 Applications

The detectability of a neutrino source as described in this paper was studied by Halzen & Hooper (2002; see also Halzen, Jacobsen & Zas 1996; Halzen & Jaczko 1996). The detection is based on the charged current interaction $\bar{\nu}_\mathrm{e} + p \rightarrow n + \mathrm{e}^+$ and the subsequent Čerenkov radiation that is emitted by the positron. An analysis based on Halzen & Jaczko (1996) shows that detection could be feasible for sources within a few Mpc for a low-background neutrino telescope.[5] This limits potential sources to our local cluster.

In the context of supernova dynamics, it has been proposed that delayed neutrino emission could revive a stalled supernova shock (Bethe & Wilson 1985). Matter that is surrounding some central, heavy object can escape if the internal energy exceeds the gravitational energy:

$$E_\mathrm{int} > E_\mathrm{grav} = \frac{GM}{D}\,, \tag{38}$$

where M is the mass of the central object and D the distance of the matter to the central object.

This material can be heated by neutrinos. We assume that the matter consists of nucleons, but for heavier nuclei similar processes can occur. Neglecting loss terms, the total energy that can be deposited by neutrinos from the central object equals

$$\Delta E = N_\mathrm{A}\sigma \frac{E^{(\nu,\,\mathrm{tot})}}{4\pi D^2}\,, \tag{39}$$

where the cross-section for neutrino capture on nucleons reads (the relevant processes and cross-sections can be found in Appendix B):

$$\sigma \sim 10^{-43}\,\mathrm{cm}^2 \times \left\langle \frac{E_\nu^2}{1\,\mathrm{MeV}^2} \right\rangle . \tag{40}$$

Following Bethe & Wilson (1985), we use the values $D = 150\,\mathrm{km}$ and $M = 1.6\,\mathrm{M}_\odot = 3 \times 10^{54}/c^2\,\mathrm{erg}$. With the expressions (34) and (35) for the neutrino flux found in this paper, we find that

$$E_\mathrm{grav} \sim 2 \times 10^{19}\,\mathrm{erg\,g^{-1}}\,, \tag{41a}$$

$$\Delta E \sim 2 \times 10^{20}\,\mathrm{erg\,g^{-1}}\,. \tag{41b}$$

We conclude that the energy released in neutrinos by the hot fireball considered here is sufficient to release material at a typical distance $D \sim 150$ km from the gravitational pull of a 1.6-$\mathrm{M}_\odot$ object.

6 CONCLUSIONS

In this paper, we have described the physics of neutrinos in a hot fireball environment. We find that the dominant neutrino processes are leptonic: neutrino creation by electron–positron annihilation and neutrino scattering off electrons and positrons.

For general initial conditions,[6] the fireball plasma is initially neutrino-opaque and the rate of neutrino creation is reasonably high. The neutrinos are in thermal equilibrium with the other components of the plasma and follow the hydrodynamical evolution of the fireball. In this evolution, the muon- and tau-neutrino decouple first, followed by the electron-neutrinos. Besides these bursts, the fireball emits neutrinos continuously in regions where it is neutrino-opaque and the creation rate is high. The effect on the evolution of the fireball and on the neutrino emission is small.

The energy spectrum of the emitted neutrinos will be approximately thermal with a temperature equal to the initial temperature of the fireball, i.e. $\langle E_\nu \rangle \sim 60$ MeV. The total energy that is emitted in (anti)neutrinos is

$$E^{(\nu,\,\mathrm{tot})} = 3.1 \times 10^{51}\,\mathrm{erg} \times \left[E_{52}^{(0)}\, R_{6.5}^{(0)}\right]^{11/16} . \tag{42}$$

A sizable fraction of the total energy of the fireball is converted into neutrinos and this fraction is not very sensitive to initial conditions. The rather limited detection possibility is mainly due to the isotropic outflow of the neutrinos, as opposed to the observed high-energy gamma-rays that originate in ultrarelativistic beamed jets in a later stage of the GRB. If the neutrinos were focused by some mechanism, detection of sources much further away could be possible. On the other hand, fewer sources will be detected because the outflow needs to be directed towards the Earth.

We have found that our initial concern that neutrino emission might prevent the production of powerful explosions from fireballs is not justified. The physical reason for this is that, for most of the parameter space where neutrino production is fast enough to cool the fireball, the fireball shields itself from cooling by being opaque to those same neutrinos. However, there may well be another snag when one considers the formation of the fireball: this requires a

[5] This is a rough signal-to-noise estimate. In particular, it assumes that there is no directional information available for triggering or reconstruction. The observational time window is 0.3 ms.

[6] These conclusions apply to fireballs that start in the neutrino-opaque region that we denoted as region I. This is the case if $(E_{0,52})^{-5/4}\,(R_{0,6.5})^{11/4} \lesssim 5$.

heating mechanism and at the start of the heating one necessarily approaches the safe zone in the lower right half of Fig. 1 from the left. Therefore, unless the heating occurs on a time-scale close to the dynamical time, the evolution track towards high energy may well get stuck in the cooling zone, causing loss of all heating energy into neutrinos. Given that the dynamical time-scale is probably the fastest thinkable heating time, it is quite possible that neutrino cooling can prevent high-energy fireballs from forming.

ACKNOWLEDGMENTS

We thank Francis Halzen, Maarten de Jong and Eli Waxman for useful discussions.

REFERENCES

Bahcall J. N., Mészáros P., 2000, Phys. Rev. Lett., 85, 1362
Baiko D. A., Yakovlev D. G., 1999, A&A, 342, 192
Beloborodov A. M., 2003, ApJ, 588, 931
Bethe H. A., Wilson J. R., 1985, ApJ, 295, 14
Bethe H. A., Applegate J. H., Brown G. E., 1980, ApJ, 241, 343
Braaten E., Segel D., 1993, Phys. Rev. D, 48, 1478
Bruenn S. W., 1985, ApJS, 58, 771
Cavallo G., Rees M. J., 1978, MNRAS, 183, 359
Dicus D. A., 1972, Phys. Rev. D, 6, 941
Dutta S. I., Ratkovic S., Prakash M., 2004, Phys. Rev. D, 69, 023005
Friman B. L., Maxwell O. V., 1979, ApJ, 232, 541
Goodman J., 1986, ApJ, 308, L47
Halzen F., Hooper D., 2002, Rep. Prog. Phys., 65, 1025
Halzen F., Jaczko G., 1996, Phys. Rev. D, 54, 2779
Halzen F., Jacobsen J. E., Zas E., 1996, Phys. Rev. D, 53, 7359
't Hooft G., 1971, Phys. Lett. B, 37, 195
Itoh N., Adachi T., Nakagawa M., Kohyama Y., Munakata H., 1989, ApJ, 339, 354
Janiuk A., Perna R., Di Matteo T., Czerny B., 2004, MNRAS, 355, 950
Kumar P., 1999, ApJ, 523, L113
Lattimer J. M., Prakash M., Pethick C. J., Haensel P., 1991, Phys. Rev. Lett., 66, 2701
Lee W. H., Ramirez-Ruiz E., Page D., 2004, ApJ, 608, L5
Mucke A., Rachen J. P., Engel R., Protheroe R. J., Stanev T., 1999, Publ. Astron. Soc. Aust., 16, 160
Munakata H., Kohyama Y., Itoh N., 1985, ApJ, 296, 197
Piran T., Shemi A., Narayan R., 1993, MNRAS, 263, 861
Prakash M., Ratkovic S., Dutta S. I., 2004, in Hong D. K., Lee C.-H., Lee H.-K., Min D.-P., Park T.-S., Rho M., eds, Proc. KIAS-APCTP Int. Symp. Astro-Hadron Phys., The Quest for New States of Dense Matter. World Scientific, Singapore, p. 476
Qian Y. Z., Woosley S. E., 1996, ApJ, 471, 331
Raffelt G. G., 1996, Stars as laboratories for fundamental physics. Univ. Press, Chicago
Ratkovic S., Dutta S. I., Prakash M., 2003, Phys. Rev. C, 67, 123002
Sehgal L. M., 1974, Nucl. Phys. B, 70, 61
Shemi A., Piran T., 1990, ApJ, 365, L55
Tubbs D. L., Schramm D. N., 1975, ApJ, 201, 467
Van Paradijs J., Kouveliotou C., Wijers R. A. M. J., 2000, ARA&A, 38, 379
Weinberg S., 1972, Gravitation and cosmology. John Wiley and Sons, Inc., New York
Woosley S. E., 1993, ApJ, 405, 273

APPENDIX A: NEUTRINO EMITTING PROCESSES

A1 Direct neutrino production

There is extensive literature on neutrino emitting processes in an electroweak plasma or in a nuclear environment. We refer the reader to Dicus (1972), Braaten & Segel (1993), Bruenn (1985), Dutta, Ratkovic & Prakash (2004), Itoh et al. (1989), Munakata et al. (1985), Ratkovic, Dutta & Prakash (2003), Baiko & Yakovlev (1999), Friman & Maxwell (1979), Lattimer et al. (1991), Qian & Woosley (1996) and further references therein for a broader overview on the subject. In the hot fireball environment, the most important processes are:

(i) photo–neutrino process, $e^{\pm} + \gamma \rightarrow e^{\pm} + \nu_i + \bar{\nu}_i$;
(ii) plasma process, $\gamma \rightarrow \nu_i + \bar{\nu}_i$;
(iii) pair annihilation, $e^- + e^+ \rightarrow \nu_i + \bar{\nu}_i$;
(iv) electron capture, $e^- + p \rightarrow n + \nu_e$; and
(v) positron capture, $e^+ + n \rightarrow p + \bar{\nu}_e$.

The last two processes constitute the non-degenerate Urca process, which is the dominant nuclear neutrino emitting process for low nucleon densities. Neutron decay is too slow to play a role of importance if the neutrons are non-degenerate.

We use the following total (i.e. adding all neutrino flavours) emissivities for the photoneutrino (Dutta et al. 2004), plasma (Ratkovic et al. 2003), pair annihilation (Itoh et al. 1989) and non-degenerate URCA (Qian & Woosley 1996) processes:

$$Q_{\rm photo} = 1.1 \times 10^{31}\ (T_{11})^9\ {\rm erg\,s^{-1}\,cm^{-3}}\,; \tag{A1a}$$

$$Q_{\rm plasma} = 7.1 \times 10^{26}\ (T_{11})^9\ {\rm erg\,s^{-1}\,cm^{-3}}\,; \tag{A1b}$$

$$Q_{\rm pair} = 3.6 \times 10^{33}\ (T_{11})^9\ {\rm erg\,s^{-1}\,cm^{-3}}\,; \tag{A1c}$$

$$Q_{\rm URCA} = 9.0 \times 10^{31}\ (T_{11})^6\,(\rho_{\rm B,8})\,{\rm erg\,s^{-1}\,cm^{-3}}\,, \tag{A1d}$$

where $\rho_{\rm B} = \rho_{\rm B,8} \times 10^8\,{\rm gr\,cm^{-3}}$. These emissivities are plotted as a function of temperature in Fig. A1. The emissivity of both the photoneutrino and the plasma process is several orders of magnitude lower than that of e^-e^+ pair annihilation, which is in keeping with similar comparisons in the literature (Itoh et al. 1989; Raffelt 1996; Prakash, Ratkovic & Dutta 2004).

Electron–positron pair annihilation and non-degenerate Urca have a different scaling behaviour with temperature, and the Urca process depends on baryon density. For the environment considered in this study, we conclude that pair annihilation is the dominant process.

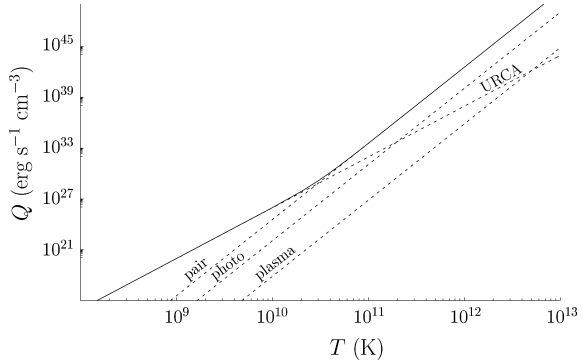

Figure A1. Neutrino emissivity of the plasma as a function of temperature. The dashed lines show the individual contributions and the solid line shows the total emissivity. We used a baryon density $\rho = 10^8\,{\rm gr\,cm^{-3}}$.

A2 Neutrinos from pion decay

Another source of neutrinos is the decay of charged pions,

(i)

$$\text{pion decay}: \quad \pi^- \rightarrow \mu^- + \bar{\nu}_\mu \rightarrow \mathrm{e}^- + \bar{\nu}_\mathrm{e} + \nu_\mu + \bar{\nu}_\mu \,,$$

and the charge-conjugate process for π^+ decay. The pions originate from photo-pion production or nucleon–nucleon (N–N) collisions:

(ii)

$$\text{photo–pion production}, \quad \gamma + n \rightarrow p + \pi^- \,, \quad \gamma + p \rightarrow n + \pi^+ \,;$$

(iii)

$$\text{N–N collisions}, \quad n + p \rightarrow p + p + \pi^- \,, \quad p + p \rightarrow n + p + \pi^+ \,.$$

The cross-section of pion production in N–N collisions ($\sigma \sim 3 \times 10^{-26}\,\mathrm{cm}^2$, see e.g. Bahcall & Mészáros 2000) is larger than that of the photo-pion process ($\sigma \sim 10^{-28}\,\mathrm{cm}^2$, see e.g. Mucke et al. 1998), but the photon density in the plasma is almost 4 orders of magnitude higher. This means that photo-pion production is the dominant pion creating process.

Pion production can only occur at energies above the pion mass threshold $E_\mathrm{t} \sim 140$ MeV. This implies that only photons in the high-energy tail of the distribution (constituting less than 5 per cent of the total energy in photons) can create pions. Most of the pions are created at the threshold and decay into muon- and electron-(anti)neutrinos with energies below $m_\mu/2 \simeq 53$ MeV. The energy spectrum of the various neutrino types is different, but the mean energies are in the range of 31 to 37 MeV.

APPENDIX B: NEUTRINO ABSORPTION AND SCATTERING PROCESSES

We summarize the cross-section formulae for the following processes:

(i) $\mathrm{e}^\pm$–neutrino scattering: $\nu_i + \mathrm{e}^\pm \rightarrow \nu_i + \mathrm{e}^\pm$;
(ii) nucleon–neutrino scattering: $\nu_i + N \rightarrow \nu_i + N$;
(iii) electron–neutrino capture: $\nu_\mathrm{e} + n \rightarrow p + \mathrm{e}^-$;
(iv) electron–antineutrino capture: $\bar{\nu}_\mathrm{e} + p \rightarrow n + \mathrm{e}^+$;

where we assume that all the particles are non-degenerate. The result, in terms of the mfp length, is plotted in Fig. B1. We use number densities $n_{\mathrm{e}^-} = n_{\mathrm{e}^+} = 1.4 \times 10^{35}\,\mathrm{cm}^{-3}$ and $n_\mathrm{B} = 5 \times 10^{31}\,\mathrm{cm}^{-3}$. From Fig. B1, we conclude that the neutrino mfp in the fireball is determined by scattering off electrons and positrons.

B1 Electron and positron scattering

The cross-section[7] for neutrino scattering off electrons in a plasma is (Tubbs & Schramm 1975):

$$\sigma = \frac{3 G_\mathrm{F}^2 \hbar^2 c^2}{2\pi} \left[(c_\mathrm{V} + c_\mathrm{A})^2 + \frac{(c_\mathrm{V} - c_\mathrm{A})^2}{3} \right] (k_\mathrm{B} T)\, E_\nu \,, \tag{B1}$$

[7] The vacuum cross-section scales as T via the neutrino energy ('t Hooft 1971; Sehgal 1974), but it is important to realize that we consider plasma cross-sections. The role of the electron mass in the vacuum cross-section is taken by the thermal energy, which leads to an increase by a factor $3.15\, k_\mathrm{B} T / m_\mathrm{e}$. For a temperature T_*, this is 2 orders of magnitude.

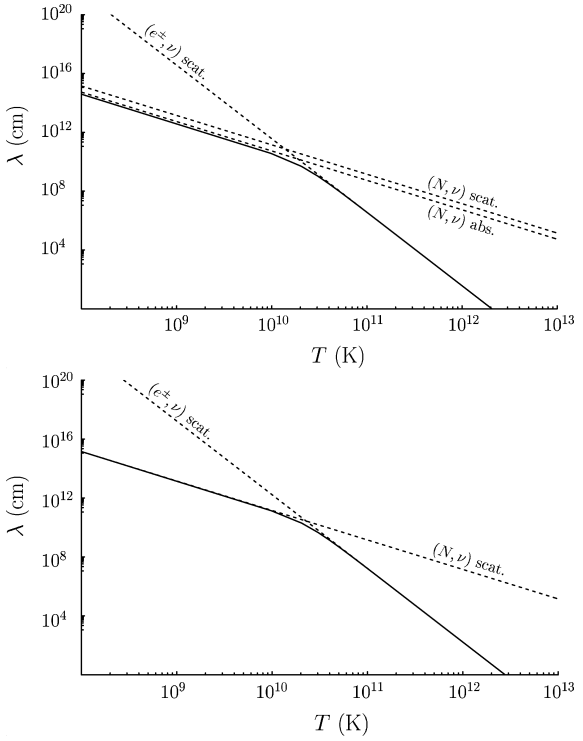

Figure B1. Neutrino mean free path lengths (cm) as a function of temperature (K). The first panel applies to electron neutrinos, and the second panel applies to muon- and tau-neutrinos. The dashed lines show the individual contributions to the mean free path length, the solid line is the combined mean free path length. We used the value $Y_\mathrm{e} = 0.5$ for nucleon scattering. The graphs for the corresponding antineutrinos are virtually identical.

where $G_\mathrm{F}^2 \hbar^2 c^2 = 5.3 \times 10^{-44}\,\mathrm{cm}^2\,\mathrm{MeV}^{-2}$ and

$$c_V = 1/2 + 2\sin^2\theta_w \,, \quad c_A = 1/2 \,, \quad \sin^2\theta_W = 0.22 \,. \tag{B2}$$

We average over a thermal neutrino distribution by replacing $E_\nu \rightarrow \langle E_\nu \rangle = 3.15\, k_\mathrm{B} T$. The formula as it stands applies to electron-neutrinos, which interact with electrons through both the charged and neutral current. For other neutrinos, one should make the following substitutions (Tubbs & Schramm 1975):

$$\begin{aligned} \nu_\mu, \nu_\tau &: c_A \rightarrow c_A - 1 \,, \quad c_V \rightarrow c_V - 1 \,; \\ \bar{\nu}_\mathrm{e} &: c_A \rightarrow -c_A \,, \quad c_V \rightarrow c_V \,; \\ \bar{\nu}_\mu, \bar{\nu}_\tau &: c_A \rightarrow 1 - c_A \,, \quad c_V \rightarrow c_V - 1. \end{aligned} \tag{B3}$$

For muon- and tau-neutrinos, this accounts for the fact that these only have a neutral interaction with electrons. The cross-section for neutrino–positron scattering is equal to the cross-section for the scattering of the corresponding antineutrino off an electron. If the electron and positron densities are equal, these processes can be combined as follows,

$$\begin{aligned} \sigma(\nu_\mathrm{i}, \mathrm{e}^\pm) &= \sigma(\nu_\mathrm{i}, \mathrm{e}^-) + \sigma(\nu_\mathrm{i}, \mathrm{e}^+) \\ &= \sigma(\nu_\mathrm{i}, \mathrm{e}^-) + \sigma(\bar{\nu}_\mathrm{i}, \mathrm{e}^-) \,, \end{aligned} \tag{B4}$$

and the mfp length due to combined electron–positron scattering follows from

$$\lambda^{-1}(\nu_\mathrm{i}, \mathrm{e}^\pm) = \sigma(\nu_\mathrm{i}, \mathrm{e}^\pm) n_{\mathrm{e}^-} \,. \tag{B5}$$

Because the electron and positron density scales as T^3, the mfp length is proportional to T^{-5}.

B2 Nucleon scattering

Neutrino–nucleon scattering is independent of neutrino flavour because the interaction is neutral. From Raffelt (1996),

$$\sigma = \frac{G_F^2 \hbar^2 c^2}{\pi} \left(C_V^2 + 3\, C_A^2\right) {E_\nu}^2 , \tag{B6}$$

where we understand that $E_\nu^2 \rightarrow \langle E_\nu^2 \rangle = 12.9(k_\mathrm{B}T)^2$. Neutrino–proton and neutrino–neutron scattering have slightly different cross-sections because of different strong interaction form factors[8] C_V and C_A. We average the cross-section by assuming an equal amount of neutrons and protons ($Y_\mathrm{e} = 0.5$),

$$\sigma\,(\nu_i, N) = \sigma\,(\nu_i,\, p) + \sigma\,(\nu_i, n)\,, \tag{B7}$$

and compute the mfp from

$$\lambda^{-1}\,(\nu_i, N) = \sigma\,(\nu_i, N)\,(0.5 n_\mathrm{B})\,. \tag{B8}$$

The baryon density is independent of temperature[9] so that the mfp length is proportional to T^{-2}.

[8] We use the values $C_V^2 = 0.0012$ (0.25) and $C_A^2 = 0.47$ (0.33) for protons (neutrons; Raffelt 1996).

[9] The baryon density does not scale with temperature in a dynamical way. Indirectly, the quantities are related by the requirement that there should be 1 TeV baryon^{-1}: a higher temperature permits a higher baryon density.

B3 Nucleon absorption

Electron-neutrinos and -antineutrinos can be absorbed by neutrons and protons through the charged interaction. The cross-section is (Tubbs & Schramm 1975)

$$\sigma = \frac{G_F^2 \hbar^2 c^2}{\pi} (3\alpha^2 + 1) {E_\nu}^2 g(E_\nu)\,, \tag{B9a}$$

$$g(E_\nu) = \left(1 \pm \frac{Q}{E_\nu}\right) \left[1 \pm 2\frac{Q}{E_\nu} + \frac{Q^2 - (\pm m_\mathrm{e}^2)}{E_\nu^2}\right]^{1/2}, \tag{B9b}$$

where $\alpha = -1.26$ is the nuclear axial coupling coefficient and $Q = 1.3$ MeV is the neutron–proton mass difference. The positive sign applies to neutrino capture on neutrons, the negative sign to antineutrino capture on protons. We do not average cross-sections here, because each process is specific to either electron-neutrinos or electron-antineutrinos. Averaging over a thermal neutrino distribution is understood as in the nucleon scattering cross-section and (up to small corrections due to the energy dependence of the function g) the mfp length is proportional to T^{-2}.

This paper has been typeset from a TEX/LATEX file prepared by the author.